Journal of AI and Data Mining
Vol 7, No 4, 2019, 487-493
DOI: 10.22044/JADM.2019.1488

Morphological Exudate Detection in Retinal Images using PCA-based Optic Disc Removal

J. Darvish and M. Ezoji*

Electrical & Computer Department, Babol Noshirvani University of Technology, Babol, Iran.

Received 23 July 2018; Revised 22 January 2019; Accepted 09 May 2019
**Corresponding author: m.ezoji@nit.ac.ir (M. Ezoji).*

Abstract
Diabetic retinopathy lesion detection such as exudate in fundus image of retina can lead to the early diagnosis of the disease. Retinal image includes dark areas such as the main blood vessels and the retinal tissue and also the bright areas such as optic disk, optical fibers, and lesions, e.g. exudate. In this paper, a multi-stage algorithm is proposed for the detection of exudate in foreground. The algorithm segments the background dark areas in the proper channels of RGB color space using morphological processing such as closing, opening, and top-hat operations. Then an appropriate edge detector discriminates between exudates and cotton-like spots or other artificial effects. To tackle the problem of optical fibers and to discriminate between these brightness and exudates, the main vessels are detected from the green channel of RGB color space. Then the optical fiber areas around the vessels are marked up. An algorithm that uses PCA-based reconstruction error is proposed to discard another fundus bright structure named optic disk. Several experiments have been performed with HEI-MED standard database and evaluated by comparing with ground truth images. These results show that the proposed algorithm has a detection accuracy of 96%.

Keywords: *Exudate Detection, Retinal Image Analysis, Diabetic Retinopathy, Biomedical Image Processing.*

1. Introduction

Retina is a thin layer of light-sensitive tissue in the back of the eye. Rays of light are focused on the retina and then the corresponding response signal is transmitted to the brain. Retinal images are widely used in ophthalmology for diagnosis of eye diseases such as Diabetic Retinopathy (DR). DR is one of the major causes of vision loss and blindness in the developed countries [1].

DR includes proliferative and non-proliferative types. It has lesion such as microaneurysms, retinal hemorrhages, exudates, cotton wool spots, neovascularization, and macular edema.

Early signs of DR and its progression can be seen in high-quality images of the retina. DR-based automated analysis can reduce the cost of diagnosis and effective treatment.

Due to the progressive nature of DR, early detection of it is very important to prevent the loss in vision. Exudate as the earliest sign of DR is the shiny yellow-white dots with sharp borders. Exudate detection in fundus images faces to challenges of variation in illumination, color, and contrast and also noise and the presence of structure such as cotton like spots and optic disk.

Several approaches have been proposed from different viewpoints to tackle the problem of exudate detection in retinal images. These research efforts can generally be classified into four main categories based on: (i) thresholding, (ii) mathematical morphology, (iii) region growing, and (iv) classification methods.

In thresholding methods, analysis is based on the local and global processing. In [1], a fuzzy function-based thresholding was used to segment the exudates. In [2], to detect the exudate boundaries, a dynamic decision thresholding method was designed.

In the second approach, specific structures are detected through a suitable morphological processing and then selected or removed [3-7]. In [3], morphological processing is combined with contrast enhancement and classification techniques. In [7], a coarse to fine strategy based

on mathematical morphology is presented for detecting exudate in color eye fundus images.
Region growing methods segment retinal image based on the spatial contiguity of neighboring pixels in various color spaces [8]. In [9], exudate was detected by fusing multiple active contours and a region-wise naive-Bayes classifier through an adaptive boosting technique.
In the fourth approach, each pixel is presented by a proper feature vector, which is formed based on the color, brightness, size, shape, edge intensity, texture, and local data set of pixels. Then to segment the exudate pixels from non-exudate pixels, machine learning techniques such as neural networks [10-13], Support Vector Machines (SVMs) [13, 14], sparse dictionary learning-based classifier [15], linear discriminant classifiers [16], naive Bayes classifier [9], and random forest algorithm [17] and fuzzy logic [18, 19] are used.
In [20], by creating the Atlas image of the healthy retinal image set, using the color difference between the atlas image and input test image, the bright lesion areas were detected.
[21] proposed a template-based method to detect the optic disc boundary followed by morphological operators, edge detector, Hough transform, and feature extraction techniques. In [22], optic disc was detected by employing an artificial neural network classifier based on the features of vessels and their background tissue.
In this paper, the background of retinal image will be removed using the morphological operations and a PCA-based optic disc detector, and then exudate areas will be separated from other bright areas with suitable edge detector.
This paper is organized as follows. The proposed algorithm is presented in Section 2. The introduction of the database, the evaluation criteria and the results of various experiments are given in Section 3. Finally, the conclusion is given in Section 4.

2. Proposed algorithm

The background and the foreground of a retina image with anatomical structures and lesions are shown in figure 1. As we can see in this figure, these components are different in sense of brightness, sharpness, size, and area and contrast. In figure 2, Channel G from RGB and Channel L from Luv color spaces are shown for a variety of retinal images. As it can be seen, in the green channel of RGB color space, background includes dark areas of the image such as main blood vessels and retinal tissue and foreground includes bright areas of the image, such as optic disk and lesions such as exudate. G-Channel is selected in most research works for foreground detection.

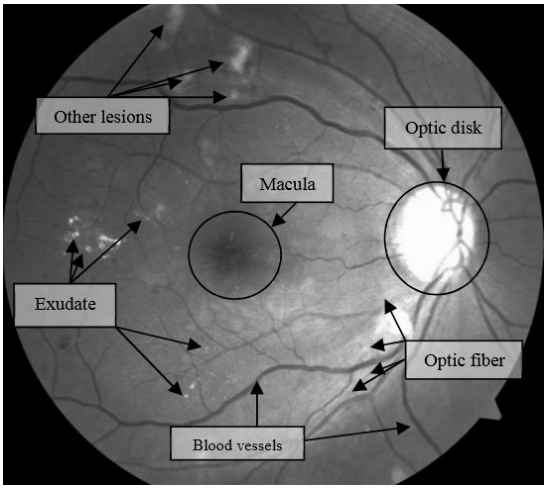

Figure 1. Retina image with anatomical structures and lesions.

In this work, various color spaces are examined to distinguish foreground from background.

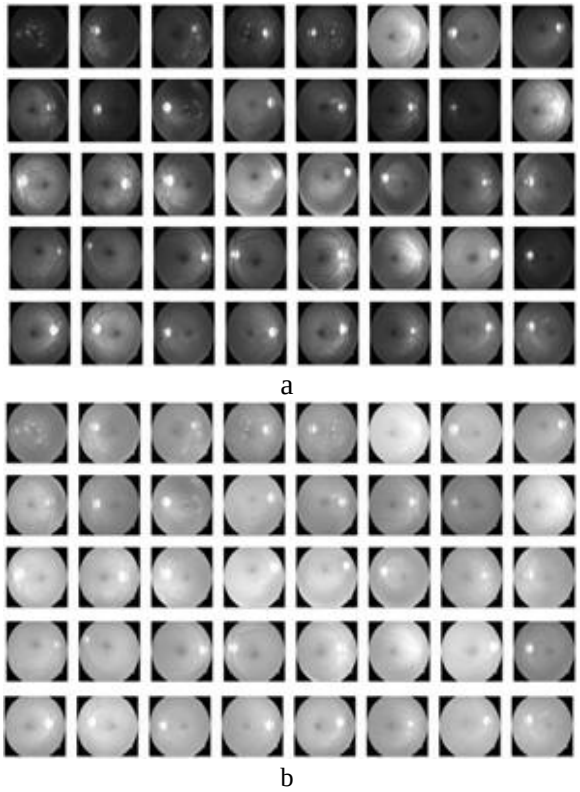

Figure 2. Retina image a) Channel G from RGB, and b) Channel L from Luv color space.

It can be seen that the overall appearance of background in L-channel is more invariant to imaging than G-channel. As a result, the channel L from CIE Luv color space is choosed.
These channels are used in two different stages of the proposed algorithm.
In this work, to reduce the effects of noise in the input retina image R_0, with an emphasis on preserving the edges, anisotropic filtering [23] was applied to the L channel. In anisotropic filtering, to

determine the new value of each pixel, neighboring pixels takes an effective role based on the similarity to that pixel in an iterative manner. Block diagram of the first step detector is shown in figure 3.

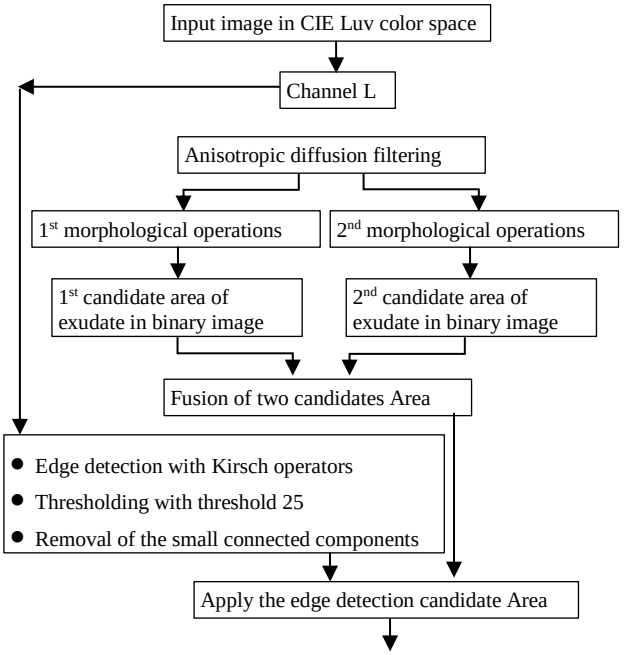

Figure 3. Block diagram of the first step of detection.

Because of different sizes of exudates, two morphological operations were applied to de-noised images. Output images of the first and second morphological operations, i.e. Z from the input image R(x,y) can be calculated as:

$$Z = sign\left(\left[\max\left\{R,\left(\left(R \bullet D_{r_1}\right)\oplus D_{r_2}\right)\right\}\right]\otimes D_{r_1}\right) \quad (1)$$

where $sign$ denotes the sign function and $\bullet$, $\oplus$ and $\otimes$ are closing, opening, and top-hat morphological operations, respectively. D_{r1} and D_{r2} are circular structural element with radius of r_1 and r_2, respectively.

There are exudates in various sizes in fundus images. Therefore, it is necessary to use the structure elements with different sizes for detecting these exudates. The size of these elements can be set using the prior knowledge about the size of the area that should be detected or removed. In this work, the size of the structure elements such as r_1 and r_2 were set empirically to achieve an acceptable detection rate.

The suitable values of r_1 for the first and second morphological operations were 20 and 100 pixels, respectively. The suitable value of r_2 for the first and second morphological operations were chosen 30 and 150 pixels, respectively. The resulting images from the first and second morphological operations were converted into binary images and then fused to highlight the exudates.

Based on the fact that exudates have sharp edges in contrast to the other retina regions, to emphasize this feature, these edges were extracted from L component using the Kirsch edge detector. After thresholding and removal of the small areas, the resulting image was used to candidate area detection.

2.1. Detection of optic disk

Candidate regions extracted from the first and second morphological operations includes optical disk, exudates, optical fibers, and other bright lesions.

In this work, we propose a PCA-based algorithm to remove the optic disc. In the blue channel of RGB color space, we crop optic disc from N images in HEI-MED database [24] into the windows with 500×500 pixels, as shown in figure 4-a. Then the PCA algorithm is applied to this set of optic discs. The vectorized principle components (PCs) are sorted in descending order of their corresponding eigenvalues and form the matrix $V = [V_1, V_2, ..., V_N]$. The first 28 corresponding PCs are illustrated in figure 4-b.

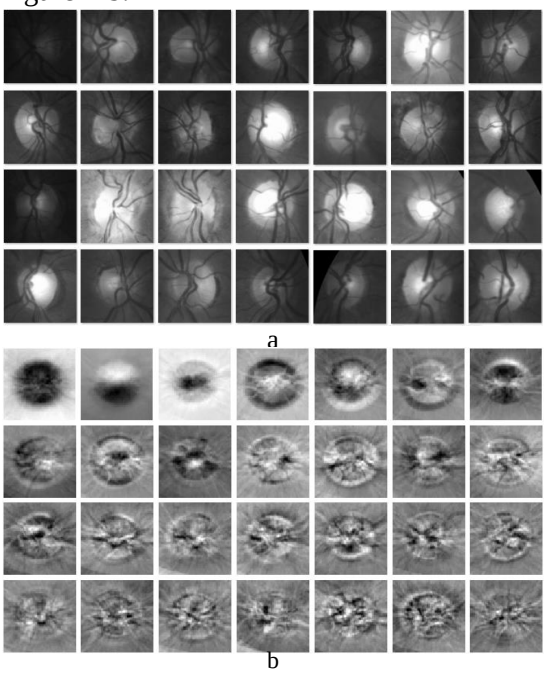

Figure 4. a) The set of the cropped optic discs from HEI-MED database , b) The first 28 corresponding

To detect the position of the optic disk in a test retinal image, we divided the image into overlapping sub-images named w with the size of 500×500 pixels.

It is known in eigenvectors decomposition that we can reconstruct w based on V_i's as $w = \bar{w} + \sum_{i=1}^{N}\left(w^T V_i\right)V_i$, where $\bar{w}$ is the mean of the subimages. The target subimage at optical disc

location can be reconstructed from k < N leading PCs in the least amount of the reconstruction error E, as follows:

$$w^* = \arg\min_{w} \left\| w - \left[\bar{w} + \sum_{i=1}^{k} \left(w^T V_i \right) V_i \right] \right\|_2 \quad (2)$$

where figure 5 illustrated this stage based on Eq. (1). In this work, k was set to 10.

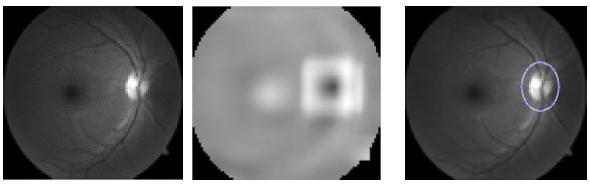

a b c

Figure 5. Optic disc detection a) Original image in blue channel, b) E matrix illustration, c) optic disk

Because of the sharp edges in the exudate area, Kirsch edge detector was applied on the candidate regions, to remove other bright areas. Thus the first step of the algorithm was held.

2.2. Main vessel detection

Bright components around the main vessels that are known as optical fibers can lead to problems in the detection process. To tackle this problem and remove these bright pixels, in the first phase, the main vessels were detected using the green channel of RGB color space. Then the areas around the vessels were marked up.

The major steps involved in detection of the main vessels are as follow:

- Anisotropic filtering to smooth the image with an emphasis on preserving edges
- Using the third morphological operations
- Main vessel detection
- 200 pixels from the left and right of main vessel are chosen to form the mask named M.

Steps related to the third morphological operations are as follow:

- Calculation of image Z from input image R:

$$Z = sign\left(\left[\max\left\{ R, \left(\left(R \bullet D_{r_1} \right) \oplus D_{r_2} \right) \right\} \right] \otimes D_{r_1} \right) \quad (3)$$

where $sign$ denotes the sign function and $\bullet$, $\oplus$ and $\otimes$ are closing, opening, and top-hat morphological operations, respectively. D_r is circular structural element with radius of r. The suitable value of r for the first and second morphological operations are 30 and 40 pixels, respectively.

- Apply the opening operation by a circular structural element with a radius of 5 pixels and then remove the connected components that are less than 200 pixels.
- The image is divided into two equal size parts of left and right. Then the part including the optical disc is kept and the other is removed.
- Two connected component with the highest number of pixels are preserved and are known as main vessels. The rest of the connected component will be discarded.

2.3. Second stage of detection

To analyze the bright areas on the mask M, the blue channel of RGB color space is used. This is due to the fact that around the main vessels is not so bright in this channel.

Block diagram of the second step detector is shown in figure 6.

Then the bright areas on the mask M from the first stage of detection, and the dark areas from the second stage detection are selected.

The following post processing steps are applied to improve the detection results:

- Remove the connected component less than 5 pixels
- Dilate morphologically with circle structural element of radius 5 pixels
- Remove optic disk from the final output image

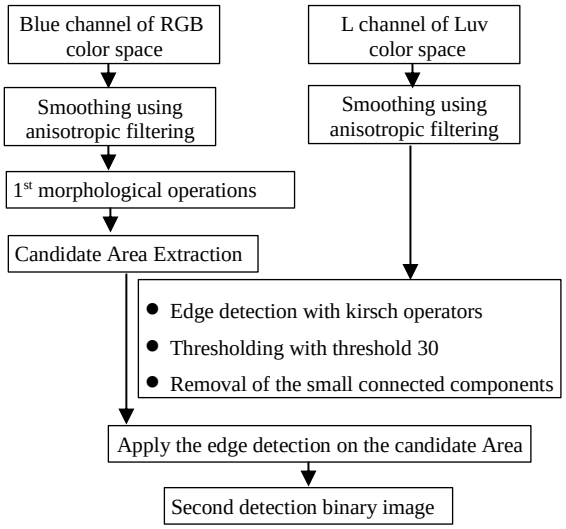

Figure 6. Block diagram of the second stage of the proposed detection algorithm.

3. Experiments and results

The proposed algorithm is evaluated on publicly available HEI-MED dataset [24]. The database includes 169 images of the retina of size 2196×1958 with the provided ground truth. Of these high resolution images, 115 images are healthy and the others contain the exudate lesions.

To evaluate the proposed algorithm, various quantitative and qualitative experiments have been performed on HEI-MED database.

Experiment-I: In this experiment, we want to show the results of various steps of the proposed

algorithm on a test image, which is shown in figure 7.

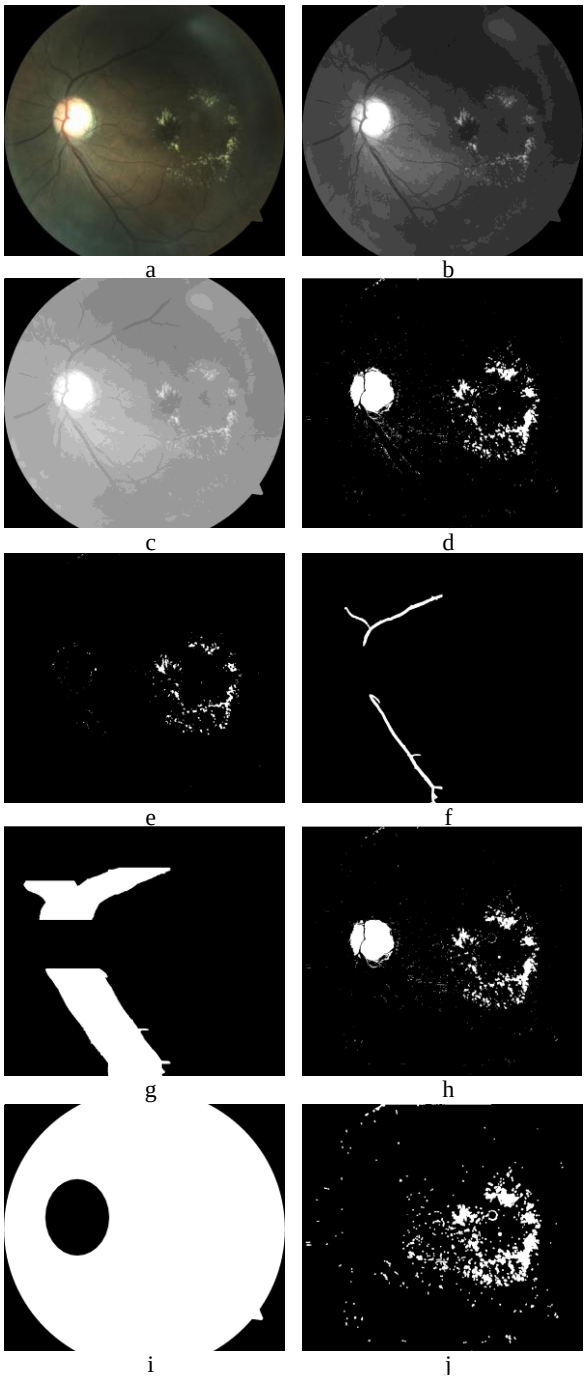

Figure 7. The results of different stages of the proposed algorithm, a) input image in RGB color space, b) green channel of RGB color space, c) L channel of Luv color space, d) result of the first stage of detection, e) result of the second stage of detection, f) the segmented main vessels, g) Mark around the main vessels (about 400 pixels), h) results of the post processing steps, i) the optic disk removing mask, j) final output of the proposed detection algorithm.

Experiment -II: We evaluate the performance of the proposed algorithm with the quantitative measurements such as sensitivity, specificity, and accuracy criteria:

$$sensitivity = \frac{TP}{TP + FN} \quad (4)$$

$$specificity = \frac{TN}{TN + FP} \quad (5)$$

$$Accuracy = \frac{TP + TN}{TP + FP + FN + TN} \quad (6)$$

where the parameters TP, FP, FN, and TN are as follow:

- TP: the number of exudate pixels that are correctly detected.
- FP: the number of non-exudate pixels that have been incorrectly identified as exudate.
- FN: the number of exudate pixels that are not detected.
- TN: the number of non-exudate pixels correctly identified as non-exudate.
-

In figure 8, the result of each above-mentioned parameter is illustrated for a test image of figure 7-a in different values of sensitivity. The result of the evaluation of the proposed algorithm is shown in table 1.

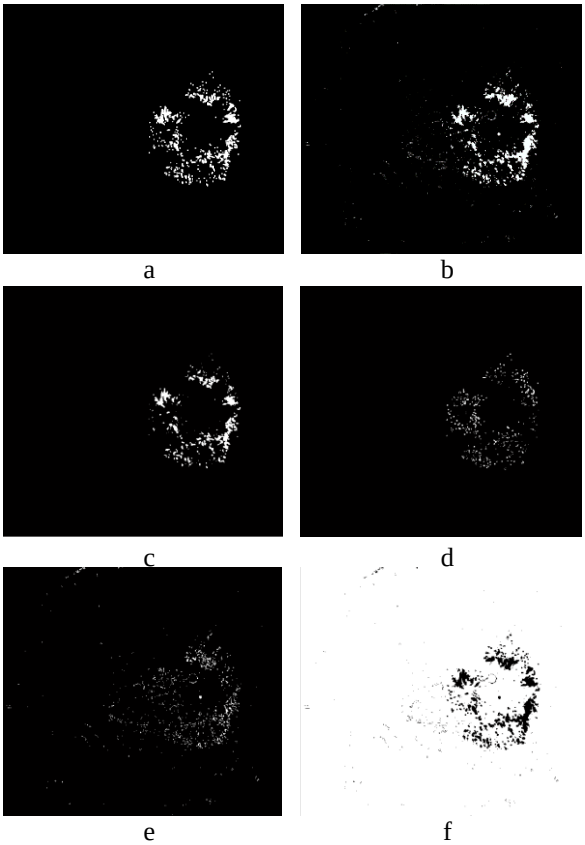

Figure 8. The results of different evaluation parameters for the test image of figure 7-a a) ground truth, b) result of the proposed algorithm, c) TP, d) FN, e) FP, and f) TN.

Table 1. The results of the proposed algorithm after the classification of the pixels as exudate and non-exudate.

	Sensitivity	Specificity	Accuracy
Proposed Algorithm	0.81	**0.96**	**0.96**
Sopharak et al.[5]*	0.65	0.90	0.82
Walter et al.[6]*	0.93	0.65	0.74
Welfer et al.[7]*	0.70	0.84	0.79
Harangi et al.[9]	0.87	0.86	0.86
Sopharak et al.[14]*	0.93	0.60	0.70
Sopharak et al.[19]*	0.91	0.68	0.75
Sanchezet al.[25]*	0.62	0.90	0.81
Jaafar et al.[26]*	0.88	0.65	0.72
Fraz et al. [27]	**0.94**	0.96	0.95
Mo et al. [28]	0.79	0.93	0.94

* indicates that these results are from [9].

The performance of the proposed algorithm is seen in table 1. We obtained a mean sensitivity of 81%, mean specificity of 96%, and accuracy of 96%.

Experiment-III: In this experiment, we compare the performance of the different approaches using the ROC curves, which is shown in figure 9. In this figure, the variation of *sensitivity* vs. *1-specificity* is plotted in different values of binarization threshold and held on the ROC curves of the other methods from [9]. For some methods cited in [9], a single (*1-specificity, sensitivity*) point is reported, which can be seen in figure 9.

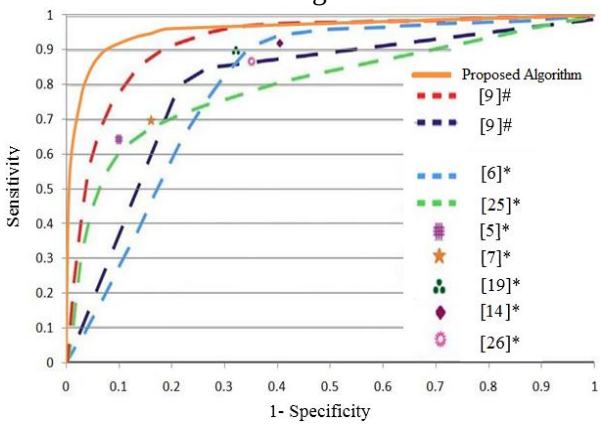

Figure 9. The ROC curve of the proposed algorithm in comparison with others from [9].

As we can see in figure 9, the performance of the proposed algorithm is superior to other algorithms in the sense of the area under the ROC.

4. Conclusion

In this paper, we proposed an algorithm for the detection of exudate in retinal images. Segmentation and removing the background areas are done using multiple morphological operations in suitable color spaces, and also with emphasis on the intensity of edges in the areas of exudate using an anisotropic filtering. Results of experiments based on HEI-MED standard database show the good performance of the proposed algorithm.

Acknowledgement

The authors acknowledge the funding support of Babol Noshirvani University of Technology through Grant program No. BNUT/389079/97-2.

References

[1] Kar, S.S. & Maity, S.P. (2018). Automatic detection of retinal lesions for screening of diabetic retinopathy, IEEE Transactions on Biomedical Engineering, vol. 65, no. 3, pp.608-618.

[2] Kaur, J. & Mittal, D. (2018). A generalized method for the segmentation of exudates from pathological retinal fundus images, Biocybernetics and Biomedical Engineering, vol. 38, no. 1, pp.27-53.

[3] Amel F., et al. (2012). Improvement of the hard exudates detection method used for computer-aided diagnosis of diabetic retinopathy, Int. J. Image, Graph. Signal Process. (IJIGSP), vol. 4, no. 4, pp. 19–27.

[4] Ravishankar S., Jain, A., & Mittal, A. (2009). Automated feature extraction for early detection of diabetic retinopathy in fundus images, in: IEEE Conference on Computer Vision and Pattern Recognition, CVPR 2009, IEEE, pp. 210–217.

[5] Sopharak A., Uyyanonvara, B., Barman, S., & Williamson, T. H. (2008). Automatic detection of diabetic retinopathy exudates from non-dilated retinal images using mathematical morphology methods, Comput. Med. Imag. Graph. vol. 32, no. 8, pp. 720–727.

[6] Walter T., Klein, J. C., Massin, P., & Erginay, A. (2002). A contribution of image processing to the diagnosis of diabetic retinopathy-detection of exudates in color fundus images of the human retina, IEEE Trans. Med. Imag., vol. 21, no. 10, pp. 1236–1243.

[7] Welfer D., Scharcanski, J., & Marinho, D. R. (2010). A coarse-to-fine strategy for automatically detecting exudates in color eye fundus images, Comput. Med. Imag. Graph., vol. 34, no. 3, pp. 228–235.

[8] Li H. & Chutatape O. (2004). Automated feature extraction in color retinal images by a model based approach, IEEE Trans. Biomed. Eng., vol. 51, no. 2, pp. 246–254.

[9] Harangi B. & Hajdu A. (2014). Automatic exudate detection by fusing multiple active contours and regionwise classification, Computers in Biology and Medicine, vol. 54, pp. 156–171.

[10] Franklin S. W. & Rajan S. E. (2013). Diagnosis of diabetic retinopathy by employing image processing technique to detect exudates in retinal images, IET Image Processing, vol. 8, no. 10, pp. 601-609.

[11] García M., Sánchez, C. I., López, M. I., Abásolo, D., & Hornero, R. (2009). Neural network based detection of hard exudates in retinal images, Comput. Methods Prog. Biomed., vol. 93, no. 1, pp. 9–19.

[12] Osareh A., Shadgar, B., & Markham, R. (2009). A computational-intelligence-based approach for

detection of exudates in diabetic retinopathy images, IEEE Trans. Inform. Technol. Biomed., vol. 13, no. 4, pp. 535–545.

[13] Khojasteh, P., Júnior, L. A. P., Carvalho, T., Rezende, E., Aliahmad, B., Papa, J. P. and Kumar, D. K. (2019). Exudate detection in fundus images using deeply-learnable features, Computers in biology and medicine, vol. 104, no. 2, pp. 62-69.

[14] Sopharak A., Dailey, M. N., Uyyanonvara, B., Barman, S., Williamson, T., Nwe, K. T., & Moe, Y. A. (2010), Machine learning approach to automatic exudate detection in retinal images from diabetic patients, J. Mod. Opt., vol.57, no. 2, pp. 124–135.

[15] Das, V. & Puhan, N. B., (2017). Tsallis entropy and sparse reconstructive dictionary learning for exudate detection in diabetic retinopathy, Journal of Medical Imaging, vol. 4, no. 2, p. 02-24.

[16] Niemeijer M., Van Ginneken, B., Russell, S. R., Suttorp-Schulten, M. S., & Abramoff, M. D. (2007). Automated detection and differentiation of drusen, exudates, and cotton-wool spots in digital color fundus photographs for diabetic retinopathy diagnosis, Invest. Ophthalmol. Vis. Sci., vol. 48, no. 5, pp. 2260–2267.

[17] Zhang X. (2014). Exudate detection in color retinal images for mass screening of diabetic retinopathy, Med. Image Anal., vol. 18, no. 7, pp. 1026–1043.

[18] Ranamuka N. G., & Meegama, R. G. N. (2013). Detection of hard exudates from diabetic retinopathy images using fuzzy logic, IET Image Process., vol. 7, no. 2, pp. 121–130.

[19] Sopharak A., Uyyanonvara, B., & Barman, S. (2009). Automatic exudate detection from nondilated diabetic retinopathy retinal images using fuzzy c-means clustering, Sensors, vol. 9, no. 3, pp. 2148–2161.

[20] Ali S., Sidibé, D., Adal, K. M., Giancardo, L., Chaum, E., Karnowski, T. P., & Mériaudeau, F. (2013). Statistical atlas based exudate segmentation, Comput. Med. Imag. Graph., vol. 37, pp. 358–368.

[21] Aquino A., et al. (2010). Detecting the optic disc boundary in digital fundus images using morphological, edge detection, and feature extraction techniques, IEEE Transactions on Medical Imaging, vol. 29, no. 11, pp. 1860-1869.

[22] Abdali-Mohammadi, & Poorshamam, A. (2018). Automatic optic disc center and boundary detection in color fundus images, Journal of AI and Data Mining, vol. 6, no 1, pp. 35-46.

[23] Perona P. & Malik J. (1990). Scale-space and edge detection using anisotropic diffusion, IEEE Trans. Pattern Anal. Machine Intell., vol. 12, no. 7, pp. 629-639.

[24] Giancardo L., et al. (2011). Automatic retina exudates segmentation without amanually labelled training set, in Proc. 2011 IEEE Int. Symp. Biomed. Imag: From Nano to Macro, Mar. 2011, pp. 1396–1400.

[25] Sánchez I., et al. (2008). A novel automatic image processing algorithm for detection of hard exudates based on retinal image analysis, Med. Eng. Phys., vol. 30, no. 3, pp. 350–357.

[26] Jaafar H. F., et al. (2010). Detection of exudates in retinal images using a pure splitting technique, in: Proceedings of the Conference of the Engineering in Medicine and Biology Society (EMBC 2010), pp. 6745–6748.

[27] Fraz, M.M., Jahangir, W., Zahid, S., Hamayun, M.M. and Barman, S.A. (2017). Multiscale segmentation of exudates in retinal images using contextual cues and ensemble classification". Biomedical Signal Processing and Control, vol. 35, no. 2, pp.50-62.

[28] Mo, J., Zhang, L. & Feng, Y. (2018). Exudate-based diabetic macular edema recognition in retinal images using cascaded deep residual networks. Neurocomputing, vol. 290, no. 5, pp.161-171.